ACS OMEGA

Open Access

http://pubs.acs.org/journal/acsodf

Article

Development of Optical Nanosensors for Detection of Potassium Ions and Assessment of Their Biocompatibility with Corneal Epithelial Cells

Hannah M. Dewey,[†] Nasif Mahmood,[†] Sofia Mariapaz Abello, Nigar Sultana, Jaron Jones, Jessica M. Gluck,* and Januka Budhathoki-Uprety*

Cite This: *ACS Omega* 2024, 9, 27338−27348

Read Online

ACCESS | Metrics & More | Article Recommendations | Supporting Information

ABSTRACT: Imbalance of potassium-ion levels in the body can lead to physiological dysfunctions, which can adversely impact cardiovascular, neurological, and ocular health. Thus, quantitative measurement of potassium ions in a biological system is crucial for personal health monitoring. Nanomaterials can be used to aid in disease diagnosis and monitoring therapies. Optical detection technologies along with molecular probes emitting within the near-infrared (NIR) spectral range are advantageous for biological measurements due to minimal interference from light scattering and autofluorescence within this spectral window. Herein, we report the development of NIR fluorescent nanosensors, which can quantitatively detect potassium ions under biologically relevant conditions. The optical nanosensors were developed by using photoluminescent single-walled carbon nanotubes (SWCNTs) encapsulated in polymers that contain potassium chelating moieties. The nanosensors, polystyrene sulfonate [PSS−SWCNTs, nanosensor 1 (NS1)] or polystyrene-*co*-polystyrene sulfonate [PS-*co*-PSS−SWCNTs, nanosensor 2 (NS2)], exhibited dose-dependent optical responses to potassium ion level. The nanosensors demonstrated their biocompatibility via the evaluation of cellular viability, proliferation assays, and expression of cytokeratin 12 in corneal epithelial cells (CEpiCs). Interestingly, the nanosensors' optical characteristics and their responses toward CEpiCs were influenced by encapsulating polymers. NS2 exhibited a 10 times higher fluorescence intensity along with a higher signal-to-noise ratio as compared to NS1. NS2 showed an optical response to potassium ion level in solution within 5 min of addition and a limit of detection of 0.39 mM. Thus, NS2 was used for detailed investigations including potassium ion level detection in serum. NS2 showed a consistent response to potassium ions at the lower millimolar range in serum. These results on optical sensing along with biocompatibility show a great potential for nanotube sensors in biomedical research.

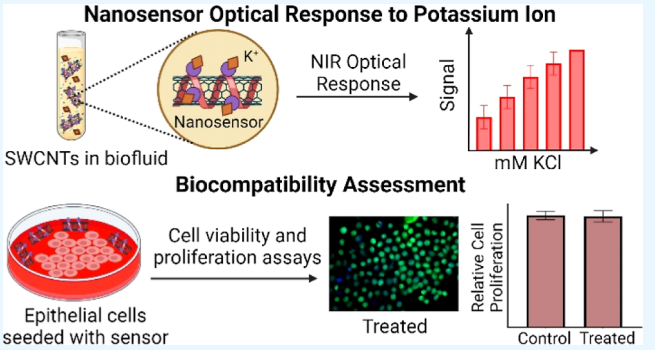

INTRODUCTION

Potassium is crucial for maintaining blood pressure, pH balance, digestion processes, activating nerve impulses, and regulating heart, muscle, kidney, neurological, and corneal functions.[1−5] Monitoring potassium-ion levels of corneal epithelium and in the ocular surface can be a useful tool in understanding ocular health. Corneal epithelium, the outermost multicellular layer of the cornea, plays an important role in the vision system by contributing to the refractive power of the eye and by acting as a protective barrier.[6] Prior research has shown that potassium ions play an important role in maintaining proliferation and apoptosis of corneal epithelial cells (CEpiCs).[7] Tear fluids which surround CEpiCs have higher concentrations of potassium ions (∼25 mM) compared to other extracellular fluids and secretions of the body.[8] An elevated presence of potassium ions protects CEpiCs from apoptosis induced by ultraviolet exposure.[8] High concentrations of potassium ions have been found to promote wound healing in mechanically scraped corneal epithelial defects in rats.[9] Different potassium-ion channels present in CEpiCs regulate the balance of potassium ions, which also play a vital role in maintaining transparency of cornea through osmotic regulation of fluid flow.[10] An imbalance in electrolyte concentration at the ocular surface and in tear fluids is considered an indicator of various ocular diseases and disorders.[11]

Methods for measuring potassium ion level in biological fluids include precipitation,[12,13] ion chromatography,[14] atomic

Received: February 26, 2024
Revised: May 9, 2024
Accepted: May 27, 2024
Published: June 11, 2024

absorption spectroscopy,[15] flame photometry,[16,17] and capillary electrophoresis.[18] Current clinical protocols use ion-selective electrodes (ISEs) to analyze biofluids for potassium.[19] ISEs utilize an ion-selective membrane, such as valinomycin, a peptide-based ionophore, which selectively binds to potassium ions and results in voltage changes in the electrode, thereby allowing for the calculation of potassium level in the solution.[19] The ISEs have been incorporated into portable platforms for point-of-care detection in biological fluids.[20] However, these devices require refrigerated storage and transport or have short shelf-lives (∼5 months)[20] which could limit the applications in fields and other resource-limited settings.

Various nanomaterials have been used in the fabrication of fluorescent nanosensors.[21,22] Interest in the optical probes for detection of potassium ion level has increased due to their simplicity and sensitivity.[23] Optical materials such as dyes and fluorophores have been developed for colorimetric and fluorescent detection of potassium ions in blood, serum, and urine samples.[24−29] These materials allow optical detection within the visible range via a turn-on response or color changes. However, detection within the visible range is less advantageous due to interference from light scattering and absorption from proteins, lipids, and nucleic acids present in biological fluids.[30,31] Detection within the near-infrared (NIR) spectral window (900−1700 nm)[37] has less light scattering and negligible autofluorescence from biological fluids and tissues.[31] Thus, NIR optical detection technology that can yield direct measurements of potassium ions could allow for measurements in native biological samples.

Semiconducting single-walled carbon nanotubes (SWCNTs) possess unique optical properties including nonphotobleaching fluorescence in the NIR region, high optical sensitivity, and high stability.[32−35] To render SWCNTs soluble in aqueous media, nanotubes can be noncovalently functionalized with polymers,[36,37] oligonucleotides,[38] small molecules,[39] and surfactants.[40] Such noncovalently functionalized SWCNT-based optical sensors have been developed for the detection of target analytes such as viruses like COVID-19 virus and[41] human immunodeficiency virus,[42] protein biomarkers,[43] quaternary ammonium compounds,[44] pH,[45] glucose,[46] and neurotransmitters.[47] These studies provide a basis for the development of targeted molecular sensors based on photoluminescent SWCNTs.

Herein, we investigated SWCNT-based optical nanosensors for the detection of potassium ion level in biological fluids and assessed the biocompatibility of these nanosensors via cell viability and proliferation assays. The nanosensors comprise photoluminescent SWCNTs, optical transducing elements wrapped within polymers that contain functionalities to effectively interact with potassium ions. The polymer-functionalized SWCNTs exhibited an optical response to potassium ions, in the presence of excess sodium ions and serum proteins, within a concentration range associated with adverse health impacts. Upon establishing that the newly developed nanosensors can detect potassium ions in a protein-rich environment, we further evaluated the biocompatibility of these nanosensors at the cellular level using mammalian CEpiCs to gain insights into potential future applications of these nanosensors in medicine and biology. In this study, interactions between CEpiCs and nanosensors were evaluated via cell viability, proliferation assays, and immunocytochemistry.

MATERIALS AND METHODS

Materials. Poly(sodium 4-styrenesulfonate) (PSS, M_w ∼ 70,000 g/mol), dimethyl sulfoxide (DMSO, anhydrous, ≥99.9%), potassium chloride (KCl), sodium chloride (NaCl), and SWCNTs (7,6) (≥90% carbon basis, 0.83 nm average diameter) chirality were purchased from Sigma-Aldrich. Poly(styrene-*co*-4-styrene sulfonic acid) (PS-*co*-PSS, M_w ∼ 11,640 g/mol) was purchased from Polymer Source, Inc., Quebec, Canada. Phosphate buffered saline (PBS) was purchased from Corning, NY, USA. Fetal bovine serum (FBS) was purchased from Atlas Biologicals, Inc., Fort Collins, CO, USA.

Nanosensor Preparation. PSS−SWCNTs were suspended in an aqueous solution by mixing 5.0 mg of PSS and 1 mg of SWCNTs in 1 mL of DI water. The mixture was then sonicated using an Ultrasonic Liquid Processor FB-505 (Fisher Scientific) in an ice bath for 10 min, 20% amplitude, pulse 30 s on/30 s off. After sonication, the suspension was centrifuged at 18.8*g* for 30 min using a Thermo Scientific Sorvall Legend Micro 21 centrifuge. The supernatant was extracted and used as the stock solution, while the residue was discarded to remove non-suspended impurities. Once the stock solution was prepared, excess polymer was removed from the PSS−SWCNT suspension by centrifugal filtration at 18.8*g* for 7 min using 100 kDa MWCO Amicon Ultra centrifugal filter units. The filtrate was discarded, and the residue was redispersed in DI water by simple mixing with a pipet, transferred into a 1.5 mL microcentrifuge tube, and stored at room temperature. PS-*co*-PSS−SWCNTs were prepared with similar methods apart from dissolving 5 mg of PS-*co*-PSS in 150 μL of DMSO first, diluting with DI water, and then adding 1 mg of SWCNTs. Sonication, centrifugation, and filtering procedures were carried out as described above.

UV−Vis NIR Spectroscopy. The absorption was measured in an Agilent Cary 5000 UV−vis−NIR spectrophotometer between 400 and 1350 nm. The concentrations of PSS−SWCNTs and PS-*co*-PSS−SWCNTs were determined by measuring the absorption of dilute samples at ∼630 nm (ε_{SWCNT} = 0.036 L mg^{-1} cm^{-1}).

Fluorescence Spectroscopy. Nanotube fluorescence was acquired via NIR fluorescence measurements with a 638 nm laser excitation source using NS MiniTracer from Applied NanoFluorescence, LLC. Parameters of 5000 ms integration and 3 averages were used for all measurements. The spectra were analyzed between 950 and 1250 nm.

Zeta Potential Measurement. PSS−SWCNT stock solution was diluted to ∼1−2 mg/L in DI water and 1 mL of solution was pipetted into a 4.5 mL poly(methyl methacrylate) cuvette. A universal "dip" cell from Malvern (product number: ZEN1002) was inserted into the cuvette, and surface charge was measured via dynamic light scattering using a Malvern Zetasizer Nano-ZS operated at 25 °C. Similar methods were carried out for surface charge measurements of PS-*co*-PSS−SWCNTs.

SWCNT Response to Potassium Ions. 100 mM, 0.50 M, and 1 M KCl solutions were added to PSS-(7,6) SWCNTs (∼103 mg/L of nanotubes) in a 1:3 v/v (KCl/SWCNT suspension) to yield final KCl concentrations of 25, 125, and 250 mM, respectively. The solution was mixed thoroughly, and NIR fluorescence was measured at a specified time upon the addition of KCl solution. Control experiments were conducted with DI water in place of a potassium chloride solution. The

https://doi.org/10.1021/acsomega.4c01867
ACS Omega 2024, 9, 27338−27348

nanotube's optical response to NaCl solution was also measured following the same methods. Sodium occurs in blood and tears alongside potassium ions at concentrations of 135−145[17] and 120−170 mM,[11] respectively. Therefore, sodium ions were tested against PSS−SWCNTs to gauge the selectivity of these nanosensors. PS-*co*-PSS−SWCNTs' (∼5 mg/L of nanotubes) response to potassium ions was evaluated by adding 5−7 mM KCl in 0.50 mM increments, and the NIR fluorescence was measured at the specified time points. Nanotube response to sodium ions was assessed with the same experimental procedures as KCl. Sensor response of PS-*co*-PSS−SWCNTs to elevated potassium- and sodium-ion levels was assessed by measuring the nanotubes' optical response to 5−7 mM KCl and 145−209 mM NaCl over time separately (1:3 v/v, KCl or NaCl/SWCNT suspension) and with a potassium and sodium ion mixture (1:1:3 v/v, KCl/NaCl/SWCNT suspension). Sensor response in protein-rich media was conducted in PBS without calcium and magnesium and in PBS with serum (10% FBS). Nanotubes were diluted in each medium type serum-free PBS or PBS with (10% FBS), the specified KCl concentration was added to the solution, and NIR fluorescence measurements were taken at specified time intervals after KCl addition. Data analysis was performed by taking the peak-to-valley difference of the (7,5) nanotube (1030−1052 nm) of each PSS−SWCNT spectrum due to background shifts while the cursor integral between 950 and 1250 nm was used for data analysis of PS-*co*-PSS−SWCNT spectra. The intensity change was calculated (if any) against the control. All experiments were performed in triplicates.

Cell Culture. Human CEpiCs (36045-16, Celprogen, Torrance, CA) were maintained in human corneal epithelial cell culture complete medium with serum (M36045-16S, Celprogen) in T-75 culture flasks coated with an FNC coating mix (0407; Athena Enzyme Service, Baltimore, MD, USA) at 37 °C and 5% CO_2. The culture medium was changed every 2−3 days. The cells were subcultured regularly using Trypsin−EDTA (0.25%) (25200072, Thermo Fisher, Waltham, MA) upon reaching approximately 80% confluence.

Cell Viability and Proliferation. For both cell viability and proliferation assays, ∼10,000 CEpiCs were plated on FNC-coated (0407, Athena Enzyme Service, Baltimore, MD) 24-well plates (142475, Thermo Fisher). PSS−SWCNTs or PS-*co*-PSS−SWCNTs were added to culture media with varying concentrations (0, 0.1, 0.2, 2, and 5 mg/L) for specified lengths of time. For day 1, PSS−SWCNT-supplemented culture media were replaced with fresh culture media after 6 h and the cells were observed after 24 h. For day 2, PSS−SWCNT- or PS-*co*-PSS−SWCNT-added culture media were replaced with fresh culture media after 24 h and observed after 48 h. Cell viability was conducted using a LIVE/DEAD Cell Imaging Kit (488/570) (R37601, Thermo Fisher) following the manufacturer's recommendations using a 1:3 dilution ratio with PBS. After removing culture media and washing with PBS once, the CEpiCs were incubated at 37 °C for 25 min with prepared solution. CEpiCs were imaged and analyzed at 10× magnification by fluorescence microscopy (EVOS FL Auto 2, Thermo Fisher). Cell proliferation assays were conducted using an alamarBlue cell viability reagent (DAL1100, Thermo Fisher) according to the manufacturer's recommendations. After incubation for 3 h with the reagent added to the culture media, the supernatant was collected from each well and transferred to a 96-well plate (10861-666, VWR, Radnor, PA) and fluorescence was measured on a microplate reader (Synergy HT, BioTek, Winooski, VT, USA) at an excitation wavelength of 540 nm and emission wavelength of 590 nm, according to the specifications of the manufacturer. For both day 1 and day 2, the obtained values were standardized to the value measured in the control group.

Immunocytochemistry. Immunocytochemistry for cytokeratin 12 (CK 12) was conducted on eight-chamber microscope slides coated with a human corneal epithelial expansion extracellular matrix (E36045-16-8MCS, Celprogen). On each chamber, 20,000 cells were plated and cultured in regular media for 24 h. At that time point, cells were then used for immunocytochemistry and fluorescent imaging using the same nanosensor concentrations and time points as done previously with cell viability and proliferation assays. Cells were fixed with 4% paraformaldehyde solution at room temperature for 20 min. Next, cells were permeabilized using 0.1% Triton X-100 for 15 min and incubated with serum blocking (2% bovine serum albumin + 2% goat serum) to block any nonspecific binding. Anti-cytokeratin 12 antibody (1:100, sc-515882, Santa Cruz Biotechnology, Dallas, TX) was diluted in blocking buffer and incubated overnight. Later, secondary antibody goat antimouse Alexa Fluor 488 (1:250, A-21141, Thermo Fisher) was diluted in 10% blocking buffer and incubated at room temperature for 1 h. Nuclei were counterstained with Hoechst 33342 (H3570, Thermo Fisher) and imaged using fluorescence microscopy (EVOS FL Auto 2, Thermo Fisher). Additionally, the number of counterstained nuclei in each chamber was counted ($n = 6$) for both day 1 and day 2 using EVOS Image Analysis software (Thermo Fisher).

Mathematical Analysis. Analysis was performed with the GraphPad Prism 9 software program (GraphPad Software, CA). Statistical analysis was conducted via two-way ANOVA with Tukey's multiple comparisons test method. Statistical significance was determined by $p < 0.05$ of differences between the means of control and treated samples: $0.01 < p < 0.05$ (*), $0.001 < p < 0.01$ (**), $0.0001 < p < 0.001$ (***), $p < 0.0001$ (****). Curve smoothing was performed via the Savitzky−Golay method. Calibration curves were calculated via simple linear regression analysis. Limits of detection (LOD) and limits of quantitation (LOQ) were calculated with the standard deviation of the regression line (σ) and the slope of the calibration curve (S). Formulas used were LOD = $3.3*(\sigma/S)$ and LOQ = $10*(\sigma/S)$.[48]

RESULTS AND DISCUSSION

Polymers with aromatic substituents and potassium-ion-binding hydrophilic moieties were chosen for SWCNT functionalization to yield water-soluble polymer−SWCNT complexes that could facilitate interactions between the SWCNTs and potassium ions in solution. Figure 1a shows the chemical structures of the polymers: poly(styrene sulfonic acid sodium salt) (PSS) and poly(styrene-*co*-styrene sulfonic acid sodium salt) (PS-*co*-PSS). Figure 1b shows the schematic of polymer−SWCNT complex formation. PSS is an FDA-approved drug used in the treatment of hyperkalemia[49] to remove excess potassium ions from the body.[50] The sulfonate group on the polymer can exchange sodium ions for potassium ions in the large intestine of the gastrointestinal tract[51,52] and the excess potassium ions along with the polymer are eliminated from the body. PSS has been found to disperse carbon nanotubes into aqueous suspension.[53] Molecular dynamic simulation studies showed that both PSS and PS-*co*-PSS can effectively interact with carbon nanotubes to form

https://doi.org/10.1021/acsomega.4c01867
ACS Omega 2024, 9, 27338−27348

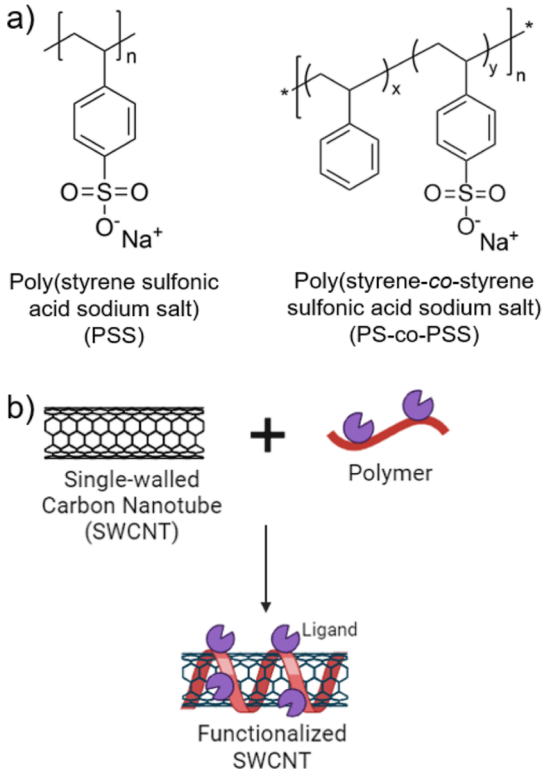

Figure 1. Schematic for nanosensor development via noncovalent functionalization of nanotubes: (a) structures of polymers used for nanotube functionalization; (b) schematic of functionalizing nanotubes with a polymer.

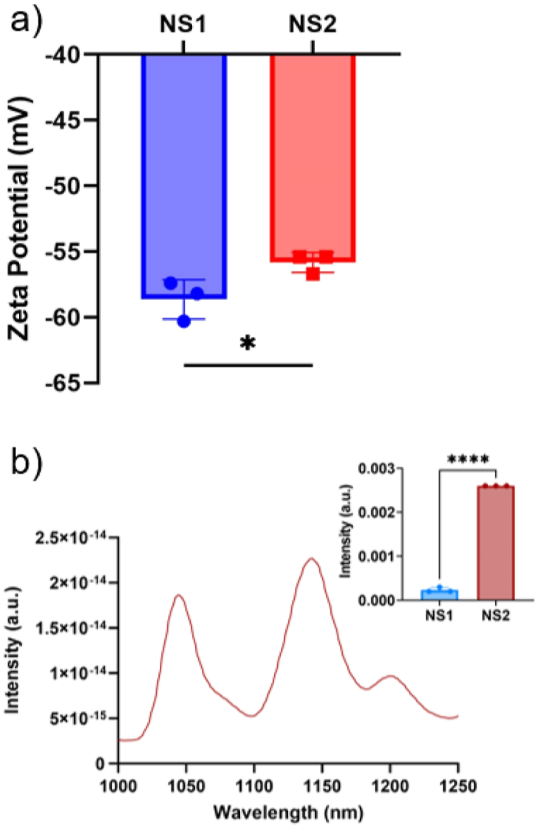

Figure 2. Characterization of NS1 (PSS−SWCNTs) and NS2 (PS-*co*-PSS−SWCNTs): (a) zeta potential of NS1 and NS2, $n = 3$; (b) NIR photoluminescence spectra of NS2 and intensity of NS1 and NS2 (inset), $n = 3$.

polymer−nanotube complexes.[54,55] The aromatic groups along the polymer backbone on PSS polymer could interact with graphitic walls of carbon nanotubes via $\pi-\pi$ interactions, and the negatively charged sulfonated groups could provide colloidal stability on resulting polymer−SWCNT complexes via electrostatic repulsion.[54] PS-*co*-PSS was chosen for nanotube functionalization due to the presence of both hydrophobic substituents and hydrophilic sulfonate groups to facilitate binding to potassium ions. The sulfonate group could act as a potassium binding agent similar to PSS, while the phenyl groups on the polymer chain could allow for hydrophobic interactions with the carbon nanotube graphitic surface.[55] Both PSS and PS-*co*-PSS could facilitate interactions between the nanotube surface and potassium ions through cation-exchange mechanisms.

Preparation and Characterization of PSS−SWCNTs and PS-*co*-PSS−SWCNTs Complexes. SWCNTs were dispersed in an aqueous solution via noncovalent functionalization with either PSS or PS-*co*-PSS polymer following literature protocol.[36] The resulting PSS−SWCNTs, denoted as nanosensor 1 (NS1), and PS-*co*-PSS−SWCNTs, denoted as nanosensor 2 (NS2), suspensions maintained their colloidal stability under ambient storage conditions for several months (>12 months). NS1 and NS2 were characterized by using UV−vis−NIR absorbance, NIR photoluminescence, and zeta potential measurements (Figures S1 and 2). Surface charges play a crucial role in stability of colloidal dispersions[56] with an absolute zeta potential of >±15 mV expected to yield stable dispersions.[57] Therefore, surface potential measurements were conducted on both nanotube suspensions to ensure a reasonable colloidal stability. Zeta potential measurements for NS1 and NS2 showed a surface charge of −58.6 ± 1.50 and −55.8 ± 0.75 mV, respectively (Figure 2a). These values are well within the criteria for colloidal stability. Furthermore, NS2 exhibited a lower negative surface potential than NS1. This can be attributed to less anionic sulfonate groups along the PSS-*co*-PS polymer chain (13 mol % degree of sulfonation) as compared to homopolymer—PSS with sulfonate groups on each repeat unit. Thus, NS2 has a lower negative charge density due to the lower degree of sulfonation on the copolymer compared with the homopolymer.

The absorption spectra of both samples (NS1 and NS2) exhibited distinct peaks in the visible and NIR region (Figure S1a) indicating E_{11} and E_{22} transitions on SWCNTs.[58] Interestingly, NS2 had more distinct E_{11} and E_{22} transitions in the absorption spectra (Figure S1a) as compared to NS1. The fluorescence measurements on NS1 exhibited a low signal, indicating that the nanotubes are highly quenched (Figure S1b), whereas NS2 had significantly enhanced the NIR signal by ∼10 folds (Figure 2b) compared to NS1 of the same nanotube concentration. The differences in absorption and emission profiles of NS1 and NS2 could be a result of the nanotube's microenvironment. It has been reported that changes in the polarity and dielectric environment near the nanotube's surface can affect their optical properties.[59,60] This can occur via solvatochromic mechanisms, where nanotube emissions can be hindered in more polar environments thereby causing a quenching effect, while emissions can be enhanced in more hydrophobic environments.[59−61] For PSS, sulfonated groups present on each repeat unit along the polymer chain

https://doi.org/10.1021/acsomega.4c01867
ACS Omega 2024, 9, 27338−27348

make it more hydrophilic compared to PS-*co*-PSS. Furthermore, the sulfonate groups are directly attached to the aromatic rings of the polymer chain which could allow for the sulfur and oxygen atoms to reside close to the nanotube surface.[54] This could attract water molecules closer to the nanotube surface thereby providing a polar microenvironment that can potentially interfere with radiative recombination of the electron−hole pair (exciton) generated upon nanotube excitation.[59,62] This would affect the optical transitions in SWCNT complexes. On the other hand, NS2 consists of nanotubes functionalized with a copolymer that only has 13 mol % degree of sulfonation resulting in higher hydrophobicity when compared to the homopolymer, PSS. Therefore, the phenyl substituents on PS-*co*-PSS on NS2 could provide a sufficiently nonpolar microenvironment which would drive some water molecules away from the nanotube surface resulting in greater absorption and emission signals.

Optical Response to Potassium Ions. Potassium chloride (KCl) solutions at various concentrations were added to NS1 and NS2 in aqueous solution, and the nanotube's optical responses were evaluated via NIR fluorescence measurements.

Response of NS1 (PSS−SWCNTs) to Potassium Ions. To evaluate the nanotube's response to potassium ions in aqueous solution, potassium chloride (KCl) solutions at various concentrations were added to an aqueous suspension of NS1 and the nanotube's optical response was measured at the specified time. NS1 showed a dose-dependent linear response with nanotubes' enhanced emission intensity (Figure 3a). The emission intensity increased over time and the strongest response occurred at 24 h with an intensity-fold increase up to 4-, 17-, and 60-fold upon addition of 25, 125, and 250 mM (final concentration) of KCl solution, respectively (Figure 3a).

The optical response from nanotubes could be attributed to sodium−potassium ion-exchange reactions on sulfonate groups on the polymer, which directly interacts with the nanotube surface. The differences in physicochemical properties between the sodium ion and potassium ion such as size and hydration could influence the vicinity of nanotubes and play a role in fluorescence enhancement. Although sodium ions are smaller than potassium ions,[63] they can attract enough water molecules to form two structured and robust hydration shells, whereas potassium ions can form a hydration shell where water molecules are distributed more broadly.[64,65] Therefore, the smaller hydrated sodium ion attached to the sulfonate groups of PSS polymer could play a role in quenching of nanotube emissions, as the hydration shells surrounding individual sodium ions could reside close to the nanotube surface.

Interactions between the nanotube surface and water have been reported to quench photoluminescence.[59,60] As sodium is exchanged for potassium ions, the larger cation can displace hydrated sodium ion−water clusters as it diffuses into the PSS−SWCNT complex. Additionally, the larger size and less stable hydration of a potassium ion compared to a sodium ion could induce dielectric changes in the microenvironment surrounding the nanotube. Changes in the dielectric environment can modulate nanotube photoluminescence through solvatochromic mechanisms.[61] Thus, the turn-on response in nanotube fluorescence could be presumably due to water displacement and charge modulation around the nanotube surface during ion-exchange interactions (Figure 3b).

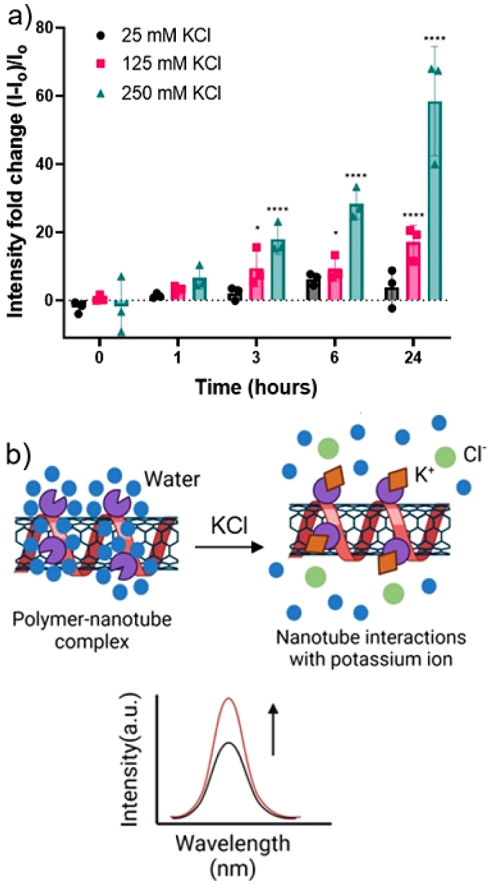

Figure 3. Optical detection of potassium ions: (a) response of NS1 to 25, 125, and 250 mM KCl via intensity-fold changes, n = 3; (b) schematic of optical detection of potassium ions with functionalized SWCNTs.

Although NS1 can respond to potassium ions in aqueous solution, the intrinsic fluorescence signal from the PSS−SWCNT complex is inherently low [Figure 2b (inset)], which necessitates a relatively higher concentration of nanotubes and potassium ions in solution to acquire measurable signals. The intrinsic low fluorescence signals from NS1 also posed challenges in data analysis. These difficulties prompted us to modify the chemical composition of the polymer dispersant to improve intrinsic photoluminescence from nanotubes. Accordingly, we developed nanosensor version 2 (NS2) in which a copolymer of PS-*co*-PSS was used instead of homopolymer PSS to encapsulate SWCNTs. We anticipated that the reduction in the number of hydrophilic and charged sulfonate moieties along the polymer chain and the introduction of aromatic phenyl substituents could modulate the optical characteristics of SWCNTs due to surface chemistry modulation. We found that a copolymer of PS-*co*-PSS with a degree of sulfonation ∼13 mol % was suitable to yield a stable suspension of SWCNTs in water with a significantly enhanced emission profile as compared to PSS-suspended SWCNTs of similar preparation.

Response of NS2 (PS-*co*-PSS−SWCNTs) to Potassium Ions in Solution. The response of NS2 to potassium ions was evaluated with similar experimental conditions as NS1 albeit at a much lower concentration of potassium ions (5−7 mM) in solution. The concentration range was chosen to mimic the serum potassium levels associated with hyperkalemia, which

https://doi.org/10.1021/acsomega.4c01867
ACS Omega 2024, 9, 27338−27348

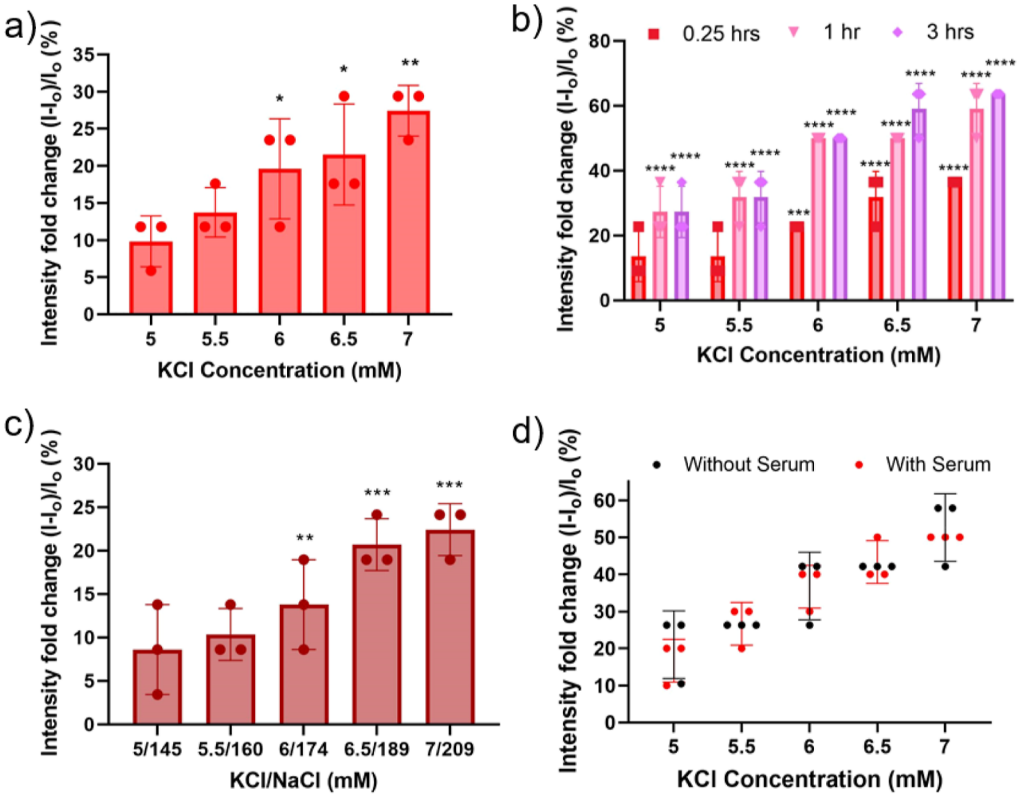

Figure 4. NS2 (PS-*co*-PSS−SWCNTs) response to potassium ions: (a) optical response of NS2 to 5−7 mM KCl in water minutes after KCl addition; (b) NS2 response to KCl over time; (c) response to the KCl/NaCl mixture with increasing concentrations of KCl in the presence of 29 folds excess of NaCl, $n = 3$; (d) response to potassium ions in PBS solution in the absence and presence of 10% FBS, $n = 3$.

occurs at 5−7 mM.[66] To evaluate the sensor response, potassium chloride salt was added to NS2 in aqueous solution, and the optical response from the nanotubes was measured via NIR fluorescence. Upon addition of KCl, a linear dose-dependent response with increase of nanotube fluorescence by 10, 14, 20, 22, and 27% at concentrations of 5, 5.5, 6, 6.5, and 7 mM, respectively, with a significant optical response at 6 mM was triggered (Figure 4a) within ∼5 min of addition of KCl solution. The LOD was 0.39 mM and LOQ was 1.19 mM (Figure S2). Furthermore, the optical response was measured over time up to 3 h upon introduction of potassium ions to nanotubes. Figure 4b shows the dose-dependent response over time with enhanced emission intensity. Upon addition of 5, 5.5, 6, 6.5, and 7 mM KCl, emission increased significantly up to 27, 32, 50, 59, and 63%, respectively, at 3 h (Figure 4b).

Sodium and potassium ions coexist in many biological systems with sodium ions found at much higher concentrations in serum (135−145 mM) and tear fluid (120−170 mM) than potassium ions. For instance, intra- and extracellular potassium-ion levels are maintained through the sodium−potassium adenosine triphosphatase pump[1,67] to regulate osmotic function, membrane potential in cells, nerve function, and muscle contractions.[67,68] Therefore, it is essential to ensure that excess sodium ions in solution do not deter the sensor's response toward recognizing potassium ions. We evaluated NS2's response to potassium in the presence of excess sodium up to 29-fold higher than potassium-ion concentration. The relative concentration ratio was selected based on their presence in biofluids. We observed that the nanotubes exhibited a dose-dependent response with increase in concentration (Figure 4c), which was consistent to NS2's response to potassium ions in the absence of sodium ions. Thus, NS2 seems to be responsive to potassium ions in the presence of excess sodium in solution.

Biological fluids, such as blood and tears, are complex and contain many proteins. One of the big challenges in the use of nanomaterials in biological environments is that proteins tend to adhere to nanomaterial surfaces affecting their functions. Oftentimes, the nanosensor's response to analytes is hindered in a protein-rich environment. Therefore, it is essential to evaluate the sensor response in protein-rich environments to gain further insights. NS2's response to potassium ions in buffer and serum was evaluated. Serum, the solution obtained after removal of blood cells and clotting factors from whole blood, is considered an important biological fluid for disease diagnosis for reduced complexity and clinical relevance.[69] Furthermore, there is considerable overlap in protein composition between blood serum and ocular biofluids including tear fluid,[70] making serum a viable model biofluid for testing the sensor's functionality in conditions similar to the ocular environment. We evaluated optical responses of NS2 to potassium ions spiked in serum diluted in PBS solution and in PBS buffer-only control. NS2 exhibited a linear dose-dependent response to KCl spiked into buffer with an emission increase up to ∼53 and 50% (at 7 mM KCl) in the absence and presence of serum, respectively (Figure 4d). Additionally, the optical response was significant to concentrations as low as 5 mM KCl. The consistent response of NS2 to KCl in serum media indicated nonsignificant interference from proteins during nanotube's interactions with potassium ions.

Biocompatibility Assessment for Nanosensors—NS1 and NS2. Biocompatibility usually refers to the quality of the

https://doi.org/10.1021/acsomega.4c01867
ACS Omega 2024, 9, 27338−27348

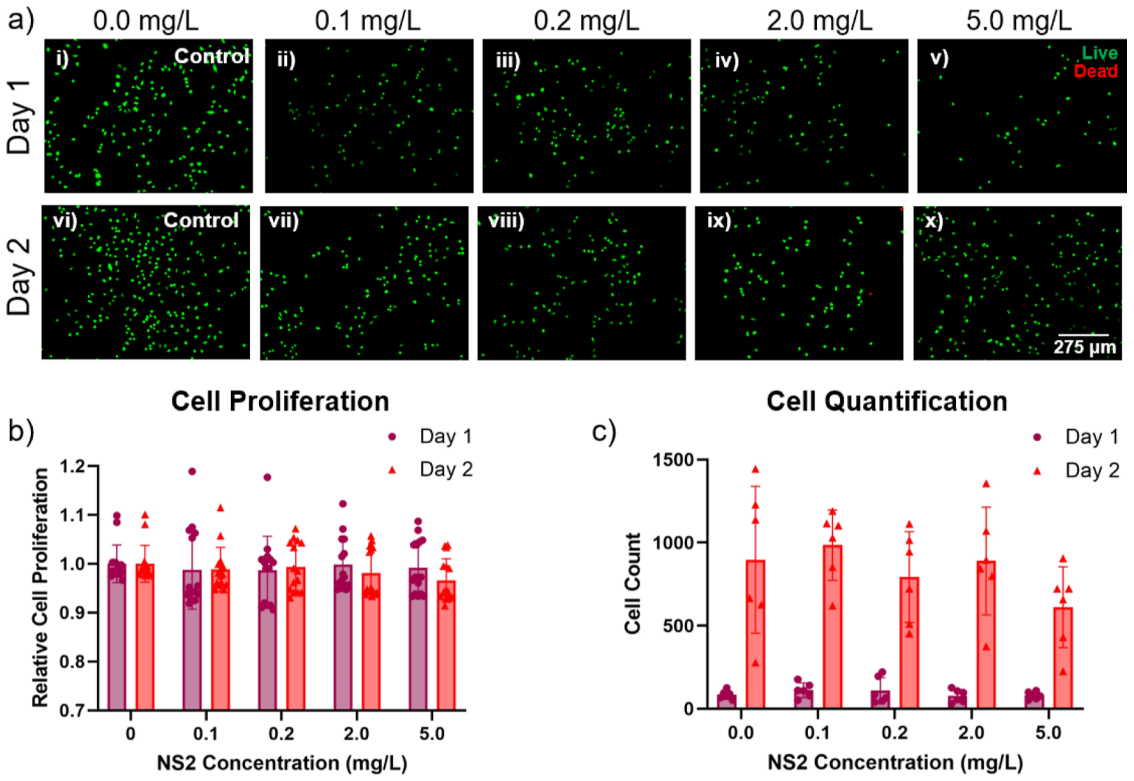

Figure 5. Cell response in the presence of the nanosensors: (a) cell viability with increasing concentrations of NS2 observed on day 1 (a, i–v) and day 2 (a, vi–x); live cells are shown in green, and dead cells are in red. Representative images are shown here. Scale bar: 275 μm. (b) Cell proliferation with increasing concentration of NS2 on day 1 and day 2 (n = 15). The values are standardized to the control. (c) Cell quantification at day 1 and day 2 in the presence of increasing concentrations of NS2 (n = 6).

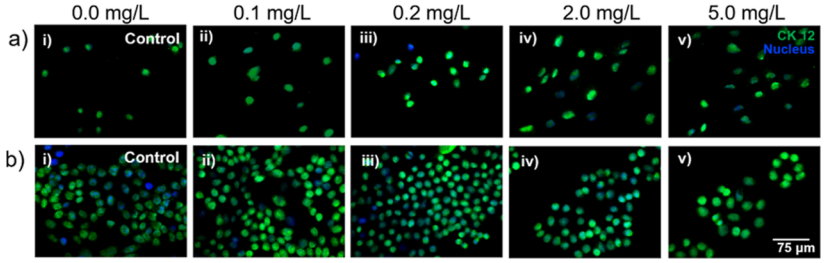

Figure 6. Expression of CK12 (green) in the presence of NS2 (PS-*co*-PSS–SWCNTs) at various concentrations observed at day 1 (a) and day 2 (b). Representative images are shown here. Scale bar: 75 μm.

tested material not having toxic or injurious effects on the biological system. Here, we define "biocompatible" as nanosensors that do not adversely affect cellular viability or proliferation capacity nor do they hinder basic CEpiC function as evidenced through expression of key functional marker cytokeratin 12. Studies suggest that surface modifications of SWCNTs can influence their interactions with cells.[71−75] In the context of this study, we compared viability, proliferation, and functionality of CEpiCs in the presence of increasing concentrations of NS1 and NS2 to analyze biocompatibility. Although NS1's optical signals were intrinsically low as compared to NS2 limiting its further applications as sensors, comparison of both these materials' response toward mammalian cells could provide insights on how surface chemistry could play a role in interactions with the cells.

Biocompatibility of the sensors with CEpiCs was evaluated using a cell viability (LIVE/DEAD) assay. The proliferation rate of CEpiCs was quantitatively determined by alamarBlue. As shown in Figure 5, the results from these assays showed that cell viability remained greater than 99% upon incubation of the cells in the presence of NS2 with an increasing nanotube concentration (0.1−5 mg/L nanotubes). For all concentrations of NS2, there was an increase in cell density between days 1 and 2 (Figure 5a). The results from proliferation assays indicate that the cells remaining adhered to the dish continue to exhibit a similar level of metabolism and thereby viability as inferred from their proliferative capacity. Also, NS2 did not cause any significant difference in cell proliferation on day 1 or day 2 compared to the control (0.0 mg/L) (Figure 5b). Additionally, cells stained with Hoechst 33342 nuclear stain were counted using EVOS image analysis software. Based on the cell count (Figure 5c), the number of cells was slightly lower at higher nanotube concentrations (5.0 mg/L) as compared to lower concentration. However, the difference was not statistically significant compared to the control (0.0 mg/L). Figure S3 shows that for all concentrations of NS1, there was an increase in cell density between day 1 and day 2 (Figure S3a) with a minimal presence of dead cells. However,

https://doi.org/10.1021/acsomega.4c01867
ACS Omega 2024, 9, 27338−27348

cell density was lower with an increase in nanotube concentration of NS1 (Figure S3). A significant decrease ($p > 0.0001$) in proliferation was observed at 5.0 mg/L concentration of NS1 compared to the control (Figure S3b). Additionally, results from counting of cells upon being stained with Hoechst 33342 nuclear stain showed that the number of cells greatly increased on day 2 compared to day 1 (Figure S3c). However, within the same day, the number of cells counted was significantly lower ($p > 0.0001$) at higher concentrations of NS1 (2.0 and 5.0 mg/L) compared to the control (0.0 mg/L).

Expression of CK12 was investigated to understand the impact of nanosensors on cell functionality and phenotype. CK12, which is uniquely expressed in CEpiCs, forms the intermediate filament framework responsible for the structural integrity and stability of the cells. The absence or mutation of CK12 can lead to weakening of the cell cytoskeleton structure and may cause Meesmann corneal dystrophy.[76] Immunocytochemistry and fluorescent imaging of CEpiCs showed that CEpiCs expressed CK12 regardless of the time of incubation and concentration of NS2 used (Figure 6). The cell morphology remained consistent, and CEpiCs formed clusters at all concentrations (Figure 6), which is an initial indication of the hallmark cellular morphology unique to CEpiCs. The CEpiC expression of CK12 remained consistent with NS1 treatment (Figure S4).

Overall, both NS1 and NS2 demonstrated their biocompatibility in a CEpiC model. CEpiCs were able to maintain proliferation and metabolic activity in the presence of both sensors, as evident from cell viability and cell proliferation assays. Functionality and phenotype of CEpiCs were ensured by the presence of the CK12 protein using immunofluorescence. This indicates that nanosensors did not adversely affect cell functionality.[77] However, we observed minimal variation in the cell response to two distinct nanosensors. The differences could be explained based on the surface chemistry on nanotubes, which is consistent to prior reports showing that surface chemistry can play a pivotal role in interactions between carbon nanotubes and cells.[78−80] The response was also concentration-dependent, with higher concentrations showing decreased metabolic activities.

CONCLUSIONS

In this study, we reported two optical nanosensors (NS1 and NS2) for the detection of potassium ions in solution and evaluated their biocompatibility in mammalian cells. NS1 was composed of SWCNTs encapsulated in PSS sodium salt polymer, and NS2 consisted of SWCNTs coated with a copolymer PS-*co*-PSS sodium salt. Tuning of nanotube's surface chemistry with two distinct polymers modulated the photophysical properties of the nanosensors, their response to the analyte (potassium ions), and interaction with mammalian cells in culture. Compared to NS1, NS2 outperformed with comparably higher emission signals than NS1, enabled detection of potassium ions at lower mM concentration, in the presence of serum proteins, and showed selective response to potassium over excess sodium ions. Furthermore, cytotoxicity assays revealed that NS2 allowed for greater cell survival at higher nanotube concentrations compared to NS1. Thus, varying the degree of sulfonation on the polymer functionalizing the nanotubes could modulate nanotube emission signals, biocompatibility, sensor sensitivity, and performance in complex environments. Nanotube-based detection of the potassium ion in biological fluids could be advantageous as an optical detection technology for precise biofluid analysis. Furthermore, future studies could utilize the knowledge gained from this research for future applications of such sensors in monitoring potassium-ion levels in biology.

ASSOCIATED CONTENT

Supporting Information

The Supporting Information is available free of charge at https://pubs.acs.org/doi/10.1021/acsomega.4c01867.

Characterization data including vis−NIR absorption spectra of SWCNTs and cell imaging and viability assays for NS1 (PDF)

AUTHOR INFORMATION

Corresponding Authors

Januka Budhathoki-Uprety − *Department of Textile Engineering, Chemistry and Science, Wilson College of Textiles, North Carolina State University, Raleigh, North Carolina 27695, United States;* orcid.org/0000-0003-3395-4823; Email: jbudhat@ncsu.edu

Jessica M. Gluck − *Department of Textile Engineering, Chemistry and Science, Wilson College of Textiles, North Carolina State University, Raleigh, North Carolina 27695, United States*; Email: jmgluck@ncsu.edu

Authors

Hannah M. Dewey − *Department of Textile Engineering, Chemistry and Science, Wilson College of Textiles, North Carolina State University, Raleigh, North Carolina 27695, United States;* orcid.org/0000-0003-1535-4605

Nasif Mahmood − *Department of Textile Engineering, Chemistry and Science, Wilson College of Textiles, North Carolina State University, Raleigh, North Carolina 27695, United States*

Sofia Mariapaz Abello − *Department of Textile Engineering, Chemistry and Science, Wilson College of Textiles, North Carolina State University, Raleigh, North Carolina 27695, United States*

Nigar Sultana − *Department of Textile Engineering, Chemistry and Science, Wilson College of Textiles, North Carolina State University, Raleigh, North Carolina 27695, United States;* orcid.org/0000-0003-4047-8212

Jaron Jones − *Department of Textile Engineering, Chemistry and Science, Wilson College of Textiles, North Carolina State University, Raleigh, North Carolina 27695, United States*

Complete contact information is available at: https://pubs.acs.org/10.1021/acsomega.4c01867

Author Contributions

†H.M.D. and N.M. contributed equally to this work. H.M.D.: conceptualization, methodology, investigation, validation, analysis, data curation, and writing—original draft and revisions; N.M.: conceptualization, methodology, investigation, analysis, data curation, and writing—original draft; S.M.A.: investigation, methodology, analysis, and writing; N.S.: investigation; J.J.: investigation; J.M.G.: supervision, writing—review and editing, and funding acquisition and resources; J.B.-U.: supervision, writing—review and editing, and funding acquisition and resources.

https://doi.org/10.1021/acsomega.4c01867
ACS Omega 2024, 9, 27338−27348

Funding

The research was partially supported by the Wilson College Research Opportunity Seed Funding program (J.M.G. and J.B.-U.), the NCSU Laboratory Research Equipment Program (J.M.G.), the Wilson College of Textiles (J.M.G. and J.B.-U.), the Department of Textile Engineering, Chemistry and Science (H.M.D., N.M., N.S., J.M.G., and J.B.-U), and the North Carolina Textile Foundation—Wilson College Fellowship (N.M.).

Notes

The authors declare no competing financial interest.

■ ACKNOWLEDGMENTS

The authors thank TECS Analytical Chemistry Laboratory and NC State Department of Materials Science Engineering Shared Characterization Facility for their help with instrumentation. Schematics and TOC graphic were created with BioRender.

■ REFERENCES

(1) Palmer, B. F.; Clegg, D. J. Physiology and pathophysiology of potassium homeostasis. *Adv. Physiol. Educ.* **2016**, *40*, 480−490.
(2) Gumz, M. L.; Rabinowitz, L.; Wingo, C. S. An Integrated View of Potassium Homeostasis. *N. Engl. J. Med.* **2015**, *373*, 60−72.
(3) Faber, E. S. L.; Sah, P. Calcium-Activated Potassium Channels: Multiple Contributions to Neuronal Function. *Neuroscientist* **2003**, *9* (3), 181−194.
(4) Weisbrod, D.; Khun, S. H.; Bueno, H.; Peretz, A.; Attali, B. Mechanisms underlying the cardiac pacemaker: the role of SK4 calcium-activated potassium channels. *Acta Pharmacol. Sin.* **2016**, *37*, 82−97.
(5) Shrimanker, I.; Bhattarai, S. *Electrolytes*. In *StatPearls*; StatPearls Publishing: Treasure Island (FL). 2024, https://www.ncbi.nlm.nih.gov/books/NBK541123/.
(6) Meek, K. M.; Knupp, C. Corneal structure and transparency. *Prog. Retin. Eye Res.* **2015**, *49*, 1−16.
(7) Roderick, C.; Reinach, P. S.; Wang, L.; Lu, L. Modulation of Rabbit Corneal Epithelial Cell Proliferation by Growth Factor-regulated K^+ Channel Activity. *J. Membr. Biol.* **2003**, *196*, 41−50.
(8) Ubels, J. L.; Van Dyken, R. E.; Louters, J. R.; Schotanus, M. P.; Haarsma, L. D. Potassium ion fluxes in corneal epithelial cells exposed to UVB. *Exp. Eye Res.* **2011**, *92*, 425−431.
(9) Ho, W.; Chiang, T.; Chang, S.; Chen, Y.; Hu, F.; Wang, I. Enhanced corneal wound healing with hyaluronic acid and high-potassium artificial tears. *Clin. Exp. Optom.* **2013**, *96*, 536−541.
(10) Lu, L. Stress-induced corneal epithelial apoptosis mediated by K^+ channel activation. *Prog. Retin. Eye Res.* **2006**, *25* (6), 515−538.
(11) Woodward, A. M.; Senchyna, M.; Argüeso, P. Differential contribution of hypertonic electrolytes to corneal epithelial dysfunction. *Exp. Eye Res.* **2012**, *100*, 98−100.
(12) Engelbrecht, R. M.; McCoy, F. A. Determination of Potassium by Tetraphenylborate Method. *Anal. Chem.* **1956**, *28*, 1772−1773.
(13) Breh, F.; Gaebler, O. H. The Determination of Potassium in Blood Serum. *J. Biol. Chem.* **1930**, *87*, 81−89.
(14) Winterberg, M.; Kirk, K. A high-sensitivity HPLC assay for measuring intracellular Na^+ and K^+ and its application to Plasmodium falciparum infected erythrocytes. *Sci. Rep.* **2016**, *6*, 29241.
(15) Qu, Z.; Steinvall, E.; Ghorbani, R.; Schmidt, F. M. Tunable Diode Laser Atomic Absorption Spectroscopy for Detection of Potassium under Optically Thick Conditions. *Anal. Chem.* **2016**, *88*, 3754−3760.
(16) Raut, S. C.; Chandel, R. S.; Abichandani, L. G. Study of Serum Electrolytes by Flame Photometer and Autoanalyser. *Sch. J. Appl. Med. Sci.* **2013**, *1*, 972−974.
(17) Kumar, V.; Gill, K. D. *To Estimate Sodium and Potassium in Serum by Using Flame Photometer*. In *Basic Concepts in Clinical Biochemistry: A Practical Guide*; Springer: Berlin, 2018; pp 147−150
(18) Nemutlu, E.; Ozaltin, N. Determination of magnesium, calcium, sodium, and potassium in blood plasma samples by capillary zone electrophoresis. *Anal. Bioanal. Chem.* **2005**, *383*, 833−838.
(19) Centers for Disease Control and Prevention. Potassium (K) in Refrigerated Serum, Potassium. 2013, https://www.cdc.gov/nchs/data/nhanes/nhanes_13_14/biopro_h_met_potassium.pdf (accessed Feb 09, 2024).
(20) Hutter, T.; Collings, T. S.; Kostova, G.; Karet Frankl, F. E. Point-of-care and self-testing for potassium: recent advances. *Sens. Diagn.* **2022**, *1*, 614−626.
(21) Cheng, Y.; Wu, J.; Cui, Y.; Zhai, J.; Wu, M.; Xie, X. Photoswitchable Temperature Nanosensors Based on the Chemical Kinetics of Photochromic Naphthopyran for Live Cell Imaging. *Anal. Chem.* **2024**, *96*, 4605−4611.
(22) Wang, L.; Zhang, Y.; Wang, L.; Cheng, Y.; Yuan, D.; Zhai, J.; Xie, X. Near-Infrared Fluoride Sensing Nano-Optodes and Distance-Based Hydrogels Containing Aluminum-Phthalocyanine. *ACS Sens.* **2023**, *8*, 4384−4390.
(23) Yin, J.; Hu, Y.; Yoon, J. Fluorescent probes and bioimaging: alkali metals, alkaline earth metals and pH. *Chem. Soc. Rev.* **2015**, *44*, 4619−4644.
(24) Sambath, K.; Liu, X.; Wan, Z.; Hutnik, L.; Belfield, K. D.; Zhang, Y. Potassium Ion Fluorescence Probes: Structures, Properties and Bioimaging. *ChemPhotoChem.* **2021**, *5*, 317−325.
(25) Song, G.; Sun, R.; Du, J.; Chen, M.; Tian, Y. A highly selective, colorimetric, and environment-sensitive optical potassium ion sensor. *Chem. Commun.* **2017**, *53*, 5602−5605.
(26) Lookadoo, D. B.; Schonhorn, J. E.; Harpaldas, H.; Uherek, C. M.; Schatz, P.; Lindgren, A.; Depa, M.; Kumar, A. A. Paper-Based Optode Devices (PODs) for Selective Quantification of Potassium in Biological Fluids. *Anal. Chem.* **2021**, *93*, 9383−9389.
(27) Kramer, J.; Kang, R.; Grimm, L. M.; De Cola, L.; Picchetti, P.; Biedermann, F. Molecular Probes, Chemosensors, and Nanosensors for Optical Detection of Biorelevant Molecules and Ions in Aqueous Media and Biofluids. *Chem. Rev.* **2022**, *122*, 3459−3636.
(28) Lee, C. H.; Folz, J.; Zhang, W.; Jo, J.; Tan, J. W. Y.; Wang, X.; Kopelman, R. Ion-Selective Nanosensor for Photoacoustic and Fluorescence Imaging of Potassium. *Anal. Chem.* **2017**, *89*, 7943−7949.
(29) Zhao, J.; Wang, W.; Cai, Q.; Wang, F.; Xie, R.; Ju, X.; Liu, Z.; Chu, L. Efficient Detection of Hyperkalemia with Highly Transparent and Ion-Recognizable Hydrogel Grating Sensors. *Ind. Eng. Chem. Res.* **2022**, *61*, 2483−2493.
(30) Hang, Y.; Boryczka, J.; Wu, N. Visible-light and near-infrared fluorescence and surface-enhanced Raman scattering point-of-care sensing and bio-imaging: a review. *Chem. Soc. Rev.* **2022**, *51*, 329−375.
(31) Cai, Y.; Wei, Z.; Song, C.; Tang, C.; Han, W.; Dong, X. Optical nano-agents in the second near-infrared window for biomedical applications. *Chem. Soc. Rev.* **2019**, *48*, 22−37.
(32) Weisman, R. B.; Kono, J. *Introduction to Optical Spectroscopy of Single-Wall Carbon Nanotubes*. In *Handbook of Carbon Nanomaterials*; World Scientific: Singapore, 2019; pp 1−43.
(33) Cheung, W.; He, H. *Carbon Nanotubes: In Vitro and In Vivo Sensing and Imaging*. In *Biosensor Nanomaterials*; John Wiley & Sons: Hoboken, 2011; pp 127−159.
(34) Kruss, S.; Hilmer, A. J.; Zhang, J.; Reuel, N. F.; Mu, B.; Strano, M. S. Carbon nanotubes as optical biomedical sensors. *Adv. Drug Delivery Rev.* **2013**, *65*, 1933−1950.
(35) Hofferber, E. M.; Stapleton, J. A.; Iverson, N. M. Review-Single Walled Carbon Nanotubes as Optical Sensors for Biological Applications. *J. Electrochem. Soc.* **2020**, *167*, 037530.
(36) Budhathoki-Uprety, J.; Jena, P. V.; Roxbury, D.; Heller, D. A. Helical Polycarbodiimide Cloaking of Carbon Nanotubes Enables Inter-Nanotube Exciton Energy Transfer Modulation. *J. Am. Chem. Soc.* **2014**, *136*, 15545−15550.
(37) Rice, N. A.; Adronov, A. Supramolecular Interactions of High Molecular Weight Poly(2,7-carbazole)s with Single-Walled Carbon Nanotubes. *Macromolecules* **2013**, *46*, 3850−3860.

https://doi.org/10.1021/acsomega.4c01867
ACS Omega 2024, 9, 27338−27348

(38) Zheng, M.; Jagota, A.; Semke, E. D.; Diner, B. A.; Mclean, R. S.; Lustig, S. R.; Richardson, R. E.; Tassi, N. G. DNA-assisted dispersion and separation of carbon nanotubes. *Nat. Mater.* **2003**, *2*, 338−342.
(39) Simmons, T. J.; Bult, J.; Hashim, D. P.; Linhardt, R. J.; Ajayan, P. M. Noncovalent Functionalization as an Alternative to Oxidative Acid Treatment of Single Wall Carbon Nanotubes with Applications for Polymer Composites. *ACS Nano* **2009**, *3*, 865−870.
(40) Moore, V. C.; Strano, M. S.; Haroz, E. H.; Hauge, R. H.; Smalley, R. E.; Schmidt, J.; Talmon, Y. Individually Suspended Single-Walled Carbon Nanotubes in Various Surfactants. *Nano Lett.* **2003**, *3*, 1379−1382.
(41) Pinals, R. L.; Ledesma, F.; Yang, D.; Navarro, N.; Jeong, S.; Pak, J. E.; Kuo, L.; Chuang, Y.; Cheng, Y.; Sun, H.; Landry, M. P. Rapid SARS-CoV-2 Spike Protein Detection by Carbon Nanotube-Based Near-Infrared Nanosensors. *Nano Lett.* **2021**, *21*, 2272−2280.
(42) Harvey, J. D.; Baker, H. A.; Ortiz, M. V.; Kentsis, A.; Heller, D. A. HIV Detection via a Carbon Nanotube RNA Sensor. *ACS Sens.* **2019**, *4*, 1236−1244.
(43) Budhathoki-Uprety, J.; Shah, J.; Korsen, J. A.; Wayne, A. E.; Galassi, T. V.; Cohen, J. R.; Harvey, J. D.; Jena, P. V.; Ramanathan, L. V.; Jaimes, E. A.; Heller, D. A. Synthetic molecular recognition nanosensor paint for microalbuminuria. *Nat. Commun.* **2019**, *10*, 3605−3609.
(44) Dewey, H. M.; Jones, J.; Lucas, S.; Hall, S.; Sultana, N.; Abello, S. M.; Budhathoki-Uprety, J. Carbon Nanotubes for Optical Detection of Quaternary Ammonium Compounds in Complex Media. *ACS Appl. Nano Mater.* **2023**, *6*, 15530−15539.
(45) Sultana, N.; Dewey, H.; Budhathoki-Uprety, J. Optical detection of pH changes in artificial sweat using near-infrared fluorescent nanomaterials. *Sens. Diagn.* **2022**, *1*, 1189−1197.
(46) Yum, K.; McNicholas, T. P.; Mu, B.; Strano, M. S. Single-Walled Carbon Nanotube-Based Near-Infrared Optical Glucose Sensors toward In Vivo Continuous Glucose Monitoring. *J. Diabetes Sci. Technol.* **2013**, *7*, 72−87.
(47) Kruss, S.; Landry, M. P.; Vander Ende, E.; Lima, B. M. A.; Reuel, N. F.; Zhang, J.; Nelson, J.; Mu, B.; Hilmer, A.; Strano, M. Neurotransmitter Detection Using Corona Phase Molecular Recognition on Fluorescent Single-Walled Carbon Nanotube Sensors. *J. Am. Chem. Soc.* **2014**, *136*, 713−724.
(48) U.S. Department of Human Health and Services. Q2(R1) Validation of Analytical Procedures: Text and Methodology Guidance for Industry; U.S. Food and Drug Administration. 2021, https://www.fda.gov/regulatory-information/search-fda-guidance-documents/q2r1-validation-analytical-procedures-text-and-methodology-guidance-industry (accessed Feb 12, 2024).
(49) Dunn, J. D.; Benton, W. W.; Orozco-Torrentera, E.; Adamson, R. T. The Burden of Hyperkalemia in Patients With Cardiovascular and Renal Disease. *Am. J. Manag. Care* **2015**, *21* (15), S307−S315.
(50) Mushiyakh, Y.; Dangaria, H.; Qavi, S.; Ali, N.; Pannone, J.; Tompkins, D. Treatment and pathogenesis of acute hyperkalemia. *J. Commun. Hosp. Int. Med. Perspect.* **2012**, *1* (4), 7372.
(51) Wong, S. W. S.; Zhang, G.; Norman, P.; Welihinda, H.; Wijeratne, D. T. Polysulfonate Resins in Hyperkalemia: A Systematic Review. *Can. J. Kid. Health Dis.* **2020**, *7*, 205435812096583.
(52) Weisberg, L. Management of severe hyperkalemia. *Crit. Care Med.* **2008**, *36* (12), 3246−3251.
(53) O'Connell, M. J.; Boul, P.; Ericson, L. M.; Huffman, C.; Wang, Y.; Haroz, E.; Kuper, C.; Tour, J.; Ausman, K. D.; Smalley, R. E. Reversible water-solubilization of single-walled carbon nanotubes by polymer wrapping. *Chem. Phys. Lett.* **2001**, *342* (3−4), 265−271.
(54) Rama, P.; Bhattacharyya, A. R.; Bandyopadhyaya, R.; Panwar, A. S. Ion Valence and Concentration Effects on the Interaction between Polystyrene Sulfonate-Modified Carbon Nanotubes in Water. *J. Phys. Chem. C* **2018**, *122*, 9619−9631.
(55) Li, L.; Cao, Q.; Liu, H.; Qiao, X.; Gu, Z.; Yu, Y.; Zuo, C. Understanding interactions between poly(styrene-co-sodium styrene sulfonate) and single-walled carbon nanotubes. *J. Polym. Sci.* **2021**, *59*, 182−190.
(56) Smith, R. J.; Lotya, M.; Coleman, J. N. The importance of repulsive potential barriers for the dispersion of graphene using surfactants. *New J. Phys.* **2010**, *12*, 125008.
(57) Sun, Z.; Nicolosi, V.; Rickard, D.; Bergin, S. D.; Aherne, D.; Coleman, J. N. Quantitative Evaluation of Surfactant-stabilized Single-walled Carbon Nanotubes: Dispersion Quality and Its Correlation with Zeta Potential. *J. Phys. Chem. C* **2008**, *112* (29), 10692−10699.
(58) Bachilo, S. M.; Strano, M. S.; Kittrell, C.; Hauge, R. H.; Smalley, R. E.; Weisman, R. B. Structure-Assigned Optical Spectra of Single-Walled Carbon Nanotubes. *Science* **2002**, *298*, 2361−2366.
(59) Silvera-Batista, C. A.; Wang, R. K.; Weinberg, P.; Ziegler, K. J. Solvatochromic shifts of single-walled carbon nanotubes in nonpolar microenvironments. *Phys. Chem. Chem. Phys.* **2010**, *12*, 6990−6998.
(60) Larsen, B. A.; Deria, P.; Holt, J. M.; Stanton, I. N.; Heben, M. J.; Therien, M. J.; Blackburn, J. L. Effect of Solvent Polarity and Electrophilicity on Quantum Yields and Solvatochromic Shifts of Single-Walled Carbon Nanotube Photoluminescence. *J. Am. Chem. Soc.* **2012**, *134*, 12485−12491.
(61) Choi, J. H.; Strano, M. S. Solvatochromism in Single-Walled Carbon Nanotubes. *Appl. Phys. Lett.* **2007**, *90*, 223114.
(62) Ohno, Y.; Iwasaki, S.; Murakami, Y.; Kishimoto, S.; Maruyama, S.; Mizutani, T. Excitonic transition energies in single-walled carbon nanotubes: Dependence on environmental dielectric constant. *Phys. Status Solidi* **2007**, *244*, 4002−4005.
(63) Freedman, J. C. *Biophysical Chemistry of Cellular Electrolytes*. In *Cell Physiology Sourcebook*; Sperelakis, N., Ed.; Academic Press, 1995; pp 3−17.
(64) Mancinelli, R.; Botti, A.; Bruni, F.; Ricci, M. A.; Soper, A. K. Hydration of Sodium, Potassium, and Chloride Ions in Solution and the Concept of Structure Maker/Breaker. *J. Phys. Chem. B* **2007**, *111*, 13570−13577.
(65) Li, H.; Francisco, J. S.; Zeng, X. C. Unraveling the mechanism of selective ion transport in hydrophobic subnanometer channels. *Proc. Natl. Acad. Sci. U.S.A.* **2015**, *112*, 10851−10856.
(66) Ahee, P.; Crowe, A. V. The management of hyperkalaemia in the emergency department. *J. Accid. Emerg. Med.* **2000**, *17*, 188−191.
(67) Strazzullo, P.; Leclercq, C. Sodium. *Adv. Nutr.* **2014**, *5*, 188−190.
(68) Seldin, D. W.; Giebisch, G. H. *The Regulation of Sodium and Chloride Balance*; Raven Press, 1990.
(69) De, M.; Rana, S.; Akpinar, H.; Miranda, O. R.; Arvizo, R. R.; Bunz, U. H. F.; Rotello, V. M. Sensing of proteins in human serum using conjugates of nanoparticles and green fluorescent protein. *Nat. Chem.* **2009**, *1*, 461−465.
(70) Ravishankar, P.; Daily, A. Tears as the Next Diagnostic Biofluid: A Comparative Study between Ocular Fluid and Blood. *Appl. Sci.* **2022**, *12*, 2884.
(71) Bianco, A.; Kostarelos, K.; Prato, M. Making carbon nanotubes biocompatible and biodegradable. *Chem. Commun.* **2011**, *47*, 10182−10188.
(72) Ferrier, D. C.; Honeychurch, K. C. Carbon Nanotube (CNT)-Based Biosensors. *Biosensors* **2021**, *11*, 486.
(73) Kumar, S.; Rani, R.; Dilbaghi, N.; Tankeshwar, K.; Kim, K. Carbon nanotubes: a novel material for multifaceted applications in human healthcare. *Chem. Soc. Rev.* **2017**, *46*, 158−196.
(74) Czarny, B.; Georgin, D.; Berthon, F.; Plastow, G.; Pinault, M.; Patriarche, G.; Thuleau, A.; L'Hermite, M. M.; Taran, F.; Dive, V. Carbon Nanotube Translocation to Distant Organs after Pulmonary Exposure: Insights from in Situ 14 C-Radiolabeling and Tissue Radioimaging. *ACS Nano* **2014**, *8* (6), 5715−5724.
(75) Gao, Z.; Varela, J. A.; Groc, L.; Lounis, B.; Cognet, L. Toward the suppression of cellular toxicity from single-walled carbon nanotubes. *Biomater. Sci.* **2016**, *4*, 230−244.
(76) Allen, E. H. A.; Courtney, D. G.; Atkinson, S. D.; Moore, J. E.; Mairs, L.; Poulsen, E. T.; Schiroli, D.; Maurizi, E.; Cole, C.; Hickerson, R. P.; James, J.; Murgatroyd, H.; Smith, F. J. D.; MacEwen, C.; Enghild, J. J.; Nesbit, M. A.; Leslie Pedrioli, D. M.; McLean, W. I.; Moore, C. T. Keratin 12 missense mutation induces the unfolded

https://doi.org/10.1021/acsomega.4c01867
ACS Omega 2024, 9, 27338−27348

protein response and apoptosis in Meesmann epithelial corneal dystrophy. *Hum. Mol. Genet.* **2016**, *25*, 1176−1191.
(77) Behzadi, S.; Serpooshan, V.; Tao, W.; Hamaly, M. A.; Alkawareek, M. Y.; Dreaden, E. C.; Brown, D.; Alkilany, A. M.; Farokhzad, O. C.; Mahmoudi, M. Cellular uptake of nanoparticles: journey inside the cell. *Chem. Soc. Rev.* **2017**, *46*, 4218−4244.
(78) Li, R.; Wang, X.; Ji, Z.; Sun, B.; Zhang, H.; Chang, C. H.; Lin, S.; Meng, H.; Liao, Y.; Wang, M.; Li, Z.; Hwang, A. A.; Song, T.; Xu, R.; Yang, Y.; Zink, J. I.; Nel, A. E.; Xia, T. Surface Charge and Cellular Processing of Covalently Functionalized Multiwall Carbon Nanotubes Determine Pulmonary Toxicity. *ACS Nano* **2013**, *7* (3), 2352−2368.
(79) Budhathoki-Uprety, J.; Harvey, J. D.; Isaac, E.; Williams, R. M.; Galassi, T. V.; Langenbacher, R. E.; Heller, D. A. Polymer cloaking modulates the carbon nanotube protein corona and delivery into cancer cells. *J. Mater. Chem. B* **2017**, *5*, 6637−6644.
(80) Sultana, N.; Dewey, H. M.; Arellano, A. G.; Budhathoki-Uprety, J. Understanding the Molecular Assemblies of Single Walled Carbon Nanotubes and Tailoring their Photoluminescence for the Next-Generation Optical Nanosensors. *Chem. Mater.* **2024**, *36* (9), 4034−4053.

https://doi.org/10.1021/acsomega.4c01867
ACS Omega 2024, 9, 27338−27348